

Respiration Physiology 120 (2000) 251-271



Effect of alveolar volume and sequential filling on the diffusing capacity of the lungs: II. Experiment

Nikolaos M. Tsoukias ^a, Donald Dabdub ^c, Archie F. Wilson ^d, Steven C. George ^{a,b,*}

a Department of Chemical and Biochemical Engineering and Materials Science, 916 Engineering Tower, University of California, Irvine. CA 92697-2575 USA

^b Center for Biomedical Engineering, University of California, Irvine, CA 92697-2575 USA
^c Department of Mechanical and Aerospace Engineering, University of California, Irvine, CA 92697-2575 USA
^d Department of Medicine, Division of Pulmonary and Critical Care, University of California, Irvine, CA 92868-4095 USA

Accepted 14 February 2000

Abstract

The diffusing capacity of the lung, DL, is a critical physiological parameter, yet the currently accepted clinical model (Jones–Meade) assumes a well-mixed alveolar region, and a constant DL independent of alveolar volume, VA, despite experimental evidence to the contrary. We have formulated a new mathematical model [Tsoukias, N.M, Wilson, A.F., George, S.C., 2000. Respir. Physiol 120, 231–249] that considers variable alveolar mixing through a single parameter, k (0 < k < 1), and a DL that is a positive function of VA (DL = a + bVA or DL = αVA^{β}). The goal of this study is to determine the suitability of this model to determine the unknown parameters a, b, α , β , and k from experimental data in normal subjects. The model predicts that the normal lung fills, in part, sequentially (k = 0.51 \pm 0.35). The following average values in all seven subjects were obtained: DLNO = $48 \cdot VA^{2/3}$ ml/min/mmHg and DLCO = $20 + 0.7 \cdot VA$ ml/min/mmHg (STPD) where VA is expressed in L (STPD). We conclude that the mathematical model is suitable for identifying the unknown parameters and thus can be used to characterize the degree of alveolar mixing (or sequential filling) as well as the volume dependence of DL. © 2000 Elsevier Science B.V. All rights reserved.

Keywords: Carbon monoxide, lung diffusing capacity; Gas exchange, diffusing capacity; Mammals, humans; Mediators, NO

1. Introduction

Mathematical modeling has been used extensively in the past to characterize and understand physiological systems including the estimation of key physiological parameters. The diffusing capacity of the lung, DL, is such a parameter with

E-mail address: scgeorge@uci.edu (S.C. George)

0034-5687/00/\$ - see front matter $\ensuremath{\mathbb{C}}$ 2000 Elsevier Science B.V. All rights reserved.

PII: S0034-5687(00)00104-3

^{*} Corresponding author. Tel.: +1-949-8243941; fax: +1-949-8242541.

significant clinical importance. Since the beginning of the century there have been numerous modeling attempts aimed at developing a simple and robust method for the accurate determination of this parameter (Krogh, 1915; Ogilvie et al., 1957; Jones and Meade, 1961; Newth et al., 1977; Cotton et al., 1979; Graham et al., 1980).

A new mathematical model was developed previously in the companion manuscript (Tsoukias et al., 2000) to determine DL for both CO and NO from a single breath constant exhalation maneuver. The model accounts for a variable alveolar axial concentration gradient due to sequential filling through the introduction of a new parameter k. In addition, the model equations were solved for a volume dependent DL. A simple linear function was assumed adequate to describe the dependence of DLCO on VA, while a simple model for the membrane diffusing capacity suggested an exponential dependence of DLNO on VA.

The goal of this manuscript is two-fold: (1) determine the suitability of the model to identify unknown parameters; and (2) compare the performance of the model to experimental data collected from normal human subjects. The suitability of the model to identify unknown parameters includes an analysis of sensitivity, identifiability, and uncertainty. Sensitivity analysis includes an investigation to determine whether the model output (i.e. exhaled concentration) is sensitive enough to the unknown parameters that need to be identified (i.e. DL). In addition, the estimated parameters can also be considered an output; thus, one may determine their sensitivity to other experimentally measured input parameters. In this way one attains a description for the error in the identifying parameters that is induced by the error in the measured inputs. Identifiability analysis determines whether or not (or under what conditions) each of the unknown parameters can be determined uniquely or identified. Uncertainty analysis utilizes the above results to predict a confidence region for the estimated parameters.

Following the model analysis, we performed a series of experimental single breath maneuvers in normal subjects. The mathematical model was then used to determine DLNO and DLCO as a function of VA, as well as the degree of mixing and/or

sequential filling in the lungs. Importantly, experimental data were also analyzed using the currently accepted Jones—Meade method (Jones and Meade, 1961) in an effort to understand the limitations and sources of error of this technique, and to highlight the advantages of our new model for accurately assessing DL.

2. Methods

2.1. Model

The model equations have been developed in detail in the companion manuscript and are presented here in a slightly different manner that will prove useful in understanding our model analysis. We will consider only the cases of variable DL and the effect of sequential filling. Thus, two distinct cases exist, and the corresponding solutions (Tsoukias et al., 2000) are as follows:

CASE I: DL = a + bVA (linear dependence, applicable to CO)

$$\begin{split} &C_{E}\!\!\left(t + \! \frac{V_{DS}}{\dot{V}_{E}}\right) \! = \\ &C_{Ao}(t)\!\!\left[\! \frac{V_{A}(t)}{V_{Ao}}\!\right]^{a\!\!\left(\frac{1}{\dot{V}_{E}} + \! \frac{k}{\dot{V}_{I}}\!\right)}\!\! e^{b\!\!\left(\frac{1}{\dot{V}_{E}} + \! \frac{k}{\dot{V}_{I}}\!\right)\!\!\left(V_{A}(t) - V_{Ao}\right)_{*}} \\ &e^{-\frac{a + bV_{Ao}}{V_{Ao}}t_{bh}} + c_{1}(k, a, b, \dot{V}_{I}, V_{RV}, V_{Ao}) \end{split} \tag{1}$$

CASE II: $D_L(V_A) = \alpha V_A^{\beta}$ (exponential dependence, applicable to NO)

$$C_{E}\left(t + \frac{V_{DS}}{\dot{V}_{E}}\right) = C_{Ao}(t)e^{\frac{\alpha}{\beta}\left(\frac{1}{\dot{V}_{E}} + \frac{k}{\dot{V}_{I}}\right)\left[V_{A}(t)^{\beta} - V_{Ao}^{\beta}\right]}e^{-\alpha V_{Ao}^{\beta} - 1_{t_{bh}}} + c_{2}(k, \alpha, \beta, \dot{V}_{I}, V_{RV}, V_{Ao})$$
(2)

where $C_E(t+V_{DS}/\dot{V}_E)$ is the exhaled concentration of gas and is equal to the concentration of the gas exiting the alveolar region at time t since the beginning of exhalation, C_{Ao} is the initial or pre-expiratory alveolar concentration, c_1 and c_2 are functions defined in the companion manuscript (Tsoukias et al., 2000), k represents an unknown parameter that varies between 0 (com-

plete alveolar mixing) and 1 (complete sequential filling), $\dot{V}_{\rm I}$ and $\dot{V}_{\rm E}$ are the inspiratory and expiratory flow rates, $t_{\rm bh}$ is the time of breathholding, and $V_{\rm RV}$ and $V_{\rm Ao}$ are the pre-inspiratory and pre-expiratory alveolar volumes. In addition, the following relationships hold:

$$C_{Ao}(t) = C_{I} \frac{C_{E,CH4}(V_{A})}{C_{I,CH4}}$$

$$= C_{I} \frac{a_{E,CH4} + b_{E,CH4}V_{A}(t)}{C_{I,CH4}}$$
(3)

$$V_{RV} = V_{Ao} - \int_{0}^{V_{Ao}} C_{E,CH4}(V_A) dV_A / C_{I,CH4}$$
 (4)

where C_I is the inspired concentration of the examined gas (CO or NO), $C_{I,CH4}$ and $C_{E,CH4}(V_A(t))$ are the inspired and exhaled concentration of the inert gas (CH₄), respectively. The decay of $C_{E,CH4}$ during exhalation is approximated as linear ($C_{E,CH4} = a_{E,CH4}V_A + b_{E,CH4}$). Thus, the model provides an expression for C_E of the form:

$$C_{E}(t) = f(t, \tilde{X}, \tilde{Y}) \tag{5}$$

where $\tilde{X} = [V_{Ao} \ \dot{V}_I \ t_{bh} \ \dot{V}_E \ C_I \ C_{I,CH4} \ a_{E,CH4}]$ represents the vector of known (experimentally measured) parameters, and $\tilde{Y} = [a \ b \ k_{CO}]$ for CO, or $\tilde{Y} = [\alpha \ \beta \ k_{NO}]$ for NO represents the vector of the unknown parameters to be identified. k_{CO} and k_{NO} represent the estimate for k using CO and NO as the test gas, respectively.

2.2. Nonlinear least squares

Identification of unknown parameters is accomplished by minimization of the sum of squares of the *absolute* error (SSE_a) between the model predictions and the experimental data:

$$SSE_{a}(\tilde{X}, \tilde{Y}) = \sum_{i} (f(t_{i}, \tilde{X}, \tilde{Y}) - C_{E}(t_{i})^{*})^{2}$$
 (6)

where $C_E(t)^*$ is the data against which the model is being compared. Minimization of the sum of squares of the *relative* error (SSE_r) is also used:

$$SSE_{r}(\tilde{X}, \tilde{Y}) = \sum_{i} \left(\frac{f(t_{i}, \tilde{X}, \tilde{Y}) - C_{E}(t_{i})^{*}}{C_{E}(t_{i})^{*}} \right)^{2}$$
(7)

Thus, the identification of the parameters reduces to the solution of one of the following unconstrained minimization problems:

$$\min_{\tilde{Y}} \{ SSE_i(\tilde{X}, \tilde{Y}) \}, \quad j = a, r$$
 (8)

The output of this minimization process is the vector of optimal parameters, \tilde{Y}_f .

In this study, we utilized a quasi-Newton optimization algorithm with line search (Kahaner et al., 1988) to determine the unknown vector \tilde{Y}_t . The model equations (Eqs. (1) and (2)) are used to generate 'experimental' data (i.e. $C_E(t)^*$). In this manner, research conclusions are independent of the specific features of a real experiment such as the intrinsic noise of the analytical instruments, the volumes and diffusing capacities of examined subjects, and the sampling rate of the data collection. However, the conclusions related to sensitivity and identifiability are still applicable to experimental data as we are investigating the intrinsic behavior of the model. Thus, the behavior of the model is examined over a wide range of potential experimental conditions and not just at the conditions of the specific experimental study. Simulations are performed for a total number of 100 data points (l = 100 where l is the number of data points) from V_{Ao} to V_{RV} with a sampling rate inversely proportional to $\dot{V}_{\rm F}$.

2.3. Sensitivity analysis

We first define the sensitivity of the model output as the gradient vector (1xn, where n is the number) of unknown parameters) of the partial derivatives of the model output (i.e. $f(t, \tilde{X}, \tilde{Y})$) with respect to the unknown parameters, estimated at the nominal parameter values \tilde{X}_o , \tilde{Y}_o . Because the unknown parameters have different absolute values, an appropriate description for the magnitude of the sensitivity is acquired by normalizing \tilde{Y} by the nominal value of the unknown parameter. In this fashion we can define the semi-relative sensitivity, $\hat{S}_{t,\tilde{Y}}(t,\tilde{X}_o,\tilde{Y}_o)$ (Frank, 1978), as:

$$\hat{S}_{f,\tilde{Y}}(t,\tilde{X}_{o},\tilde{Y}_{o}) = \left[\frac{\partial f(t,\tilde{X},\tilde{Y})}{\partial Y_{j}}Y_{oj}\right]_{\tilde{X}_{o},\tilde{Y}_{o}} \quad j = 1,...n$$
(9)

Each element of the matrix represents the absolute change of the model's output per fractional (or relative) change of the corresponding parameter. Thus, sensitivities with respect to different parameters can be compared. The unknown parameters must significantly effect the model output in order to be identified. Thus, the change in the model's output for an acceptable perturbation in any of the parameters (i.e. parameter induced error (Frank, 1978)) must be significant. A necessary criterion for the sensitivity analysis is that this parameter induced error must be larger than the intrinsic error of the analytical instrument used to measure $C_E(t)^*$.

The behavior of the model needs to be examined at different nominal points \tilde{X}_o , \tilde{Y}_o (i.e. points in the (n+m)-dimensional space) in order to determine experimental conditions that are particularly desirable (high $\hat{S}_{f,\ \tilde{Y}}$) or undesirable (low $\hat{S}_{f,\ \tilde{Y}}$). Thus, a root mean square semi-relative sensitivity function is defined to represent a sensitivity index over the entire examined portion of the exhalation:

$$\bar{\hat{S}}_{f, \ \tilde{Y}}(\tilde{X}_{o}, \ \tilde{Y}_{o}) = \sqrt{\frac{\sum_{t} (\hat{S}_{f, \ \tilde{Y}}(t, \ \tilde{X}_{o}, \ \tilde{Y}_{o}))^{2}}{l}}$$
(10)

where the summation term includes l time points in the examined exhalation interval. Maximizing this index provides the optimal experimental conditions for the estimation of a single parameter (Y_i) when the output (C_E) has an additive, zero mean, constant variance, and independent normal error, and the independent variables (\tilde{X}) are errorless (Beck and Arnold, 1977). In the analysis above we have assumed errorless measured input parameters (\tilde{X}) . However, significant error may be associated with the measurement of any of these parameters. The analysis of potential error in \tilde{X} exceeds the scope of this study and has been previously presented (Tsoukias, 1999).

2.4. Identifiability analysis

There are different problems that might occur during the process of identifying unknown parameters, such as the existence of local minima in SSE, or multiple global minima. Depending on the initial estimation of the unknown parameters, the algorithm might converge to a local minimum, resulting in an error. This problem can be overcome by utilizing a better initial estimate. The presence of multiple global minima renders a unique \tilde{Y}_f unidentifiable. This constitutes a more serious threat for the suitability of the model, and is the focus of our analysis.

We can utilize the sensitivity-based local-identifiability method (Beck and Arnold, 1977). This method states simply that two parameters are locally unidentifiable (cannot be distinguished from each other) if their sensitivities (i.e. $\hat{S}_{f, \tilde{Y}}$) are linearly dependent (analysis not shown here, see (Tsoukias, 1999)). This method is useful for identifying whether or not two parameters can be distinguished from one another locally. However, it does not address the issue of global unidentifiability.

Our approach is to construct three-dimensional images of SSE with respect to any two of the unknown parameters, while minimizing for the third. These three-dimensional maps of SSE reveal the uniqueness of a potential global minimum in the examined range of parameter values. In addition, the contours of SSE define confidence regions for the identifying parameters and can be used to provide a description for the uncertainty of the estimated parameters (see uncertainty analysis below).

2.5. Uncertainty analysis

The *F*-statistic test as described by Beck and Arnold can be used to attain confidence contours for the estimated parameters (Beck and Arnold, 1977). Assuming additive, zero mean, and normal distributed measurement errors, and errorless measured inputs, the following relationship applies:

$$F_{1-a}(n, l-n) = \frac{\text{SSE}(\tilde{\mathbf{Y}}) - \text{SSE}(\tilde{\mathbf{Y}}_f)}{\text{SSE}(\tilde{\mathbf{Y}}_f)} \frac{(l-n)}{n}$$
 (11)

Thus, all combinations of the estimated parameter values that produce SSE within a range around the minimum value, based on the confidence level $(1-\alpha)$, are potential optimal points. Thus, the three-dimensional maps of SSE can be translated to confidence regions for the estimated parameters. The range of potential optimal values for the parameters, and thus the uncertainty of the esti-

mation, will depend on the magnitude of the sensitivity and on the local identifiability of the parameters in relationship with the accuracy of the least square fitting (SSE(\tilde{Y}_t)).

2.6. Estimating the derivatives

The partial derivatives in $\hat{S}_{f, \tilde{Y}}$ cannot be estimated analytically due to the complex form of Eqs. (1) and (2); thus, numerical techniques are employed. The partial derivatives were estimated using automatic differentiation techniques. These techniques are based on the application of the chain rule, over the composition of elementary operations, used for the computation of a function. We used the ADIFOR 2.0 system for automatic differentiation of FORTRAN code (Bischof et al., 1994). The system performs a symbolic source transformation of the FORTRAN code (i.e. rewrites the original code) inserting statements for the computation of first order derivatives according to the automatic differentiation techniques. In the end, the generated code provides the original output plus a user-specified Jacobian matrix of partial derivatives. ADIFOR-

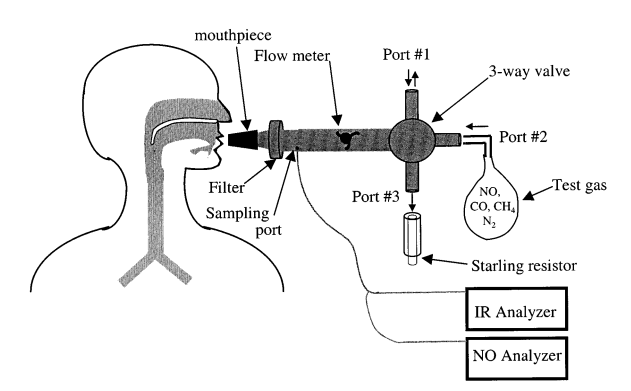


Fig. 1. Schematic of experimental set-up. The mouthpiece between the subject's mouth and sampling port comprises the expiratory dead space $V_{\rm DS,exp}$ (100 ml), while the space between the sampling port and the test gas compromise the inspiratory dead space $V_{\rm DS,insp}$ (150 ml), and includes a flow meter and a three-way valve. The valve is controlled electronically allowing the subjects to tidal breath room air through port 1, make a single inspiration of the test gas through port 2, and then exhale through port 3. A starling resistor was placed on port 3 to facilitate a constant slow expiratory flow independent of the expiratory effort of the subject.

generated code outperforms finite difference approximation both in accuracy and computational time.

2.7. Subjects

Single breath maneuvers were performed in seven normal men $(28.4 \pm 3.8 \text{ (SD)})$ yr; $160 \pm 30 \text{ (SD)}$ pounds) with no history of smoking or lung diseases. The protocol was approved by the Institutional Review Board at the University of California, Irvine. Subjects were categorized as normal on the basis of standard spirometry that included forced vital capacity, forced expiratory volume in 1 sec, and forced expiratory flow between 25 and 75% of the exhaled volume.

2.8. Experimental setup

The general principles of the experimental setup are presented schematically in Fig. 1. The mouthpiece (Sensormedics, Yorba Linda, CA) between the subject's mouth and sampling port comprises the expiratory dead space $V_{DS,exp}$ (100 ml), while the space between the sampling port and the test gas compromise the inspiratory dead space V_{DS,insp} (150 ml), and includes a flow meter and a three-way valve. The valve was controlled electronically allowing the subjects to tidal breath room air through port 1, make a single inspiration of the test gas through port 2, and then exhale through port 3. A Starling resistor was placed on port 3 to facilitate a constant slow expiratory flow independent of the expiratory effort of the subject.

2.9. Airstream analysis

NO concentration was measured using a chemiluminescence NO analyzer (NOA280, Sievers Instruments, Boulder, CO). The instrument provides highly accurate (repeatability ± 1 ppb) gas phase measurements with a very small detection threshold (< 5 ppb-500 ppm) and a fast response time (0-90% 200 ms). A needle valve restricts flow and maintains an operating reaction cell pressure of 7.5 mmHg and a sampling rate 250 ml/min. Calibration of the instrument was per-

formed on a daily basis using a certified NO gas mixture (45 ppm in N_2) (Scott Medical Products, Plumsteadville, PA) and a purified filter (Sievers, Boulder, CO) for the zero point calibration.

The measurement of CO, CH₄, flow rate and the operation of the valves were performed by Sensormedics 2200 pulmonary function equipment (Sensormedics, Anaheim, CA). The equipment utilizes a fast-response multi-gas infrared analyzer and a mass flow sensor. Calibration of the infrared analyzer, and the flow meter, was done on a daily basis using our test gas (see below) and a three-liter syringe.

2.10. Gas mixtures

Two different mixtures were used as the inspired test gas; one with and one without NO. The NO-free mixture contained 0.3% CO, 0.3% CH_4 , 0.3% C_2H_2 , and 21% O_2 in N_2 (Puritan Bennet, Overland Park, KS). The second test gas was identical to the first with the exception of 50 ppm NO. This gas was generated by mixing equal volumes in a mylar bag of a gas containing 6% CO, 6% CH₄, 6% C₂H₂ and 42% of O₂ in N₂ (Scott Medical Products, Plumsteadville, PA) with a gas containing 100 ppm of NO in N₂ (INOMAX, Ohmeda, CA). The gas was mixed just prior to each single breath test to avoid significant levels of NO₂ from the oxidation of NO (Borland and Higenbottam, 1989). The NO-free gas was used as a control to determine the potential effect of NO on the simultaneous determination of D_{LCO} . The addition of acetylene in the mixture was for the simultaneous estimation of cardiac output and tissue volume (data not shown here) (Martonen and Wilson, 1982).

2.11. Protocol

Subjects performed a series of single breath maneuvers in a sitting position. A minimum time of 4 min was allowed to elapse between the tests to allow the inspired test gas to wash out from the patient's lungs. The subjects were allowed to tidal breath room air through a mouthpiece, and then instructed to exhale to residual volume before performing the single breath maneuver (ATS, 1987). The subjects then performed a rapid inspiration of the test gas followed by one of two different single breath maneuvers: (1) a constant exhalation maneuver whereby the subject exhales until RV with a constant low flow rate after a short period of breathholding (≈ 0.5 sec); and (2) a prolonged breathhold maneuver whereby the subject exhales rapidly following a significant breathhold (≈ 6 sec). Our breathhold time was somewhat shorter that the standard method (\approx 10 sec) in order to preserve a high end-exhaled NO concentration (i.e. much larger than endogenous levels) (Guenard et al., 1987; Borland and Higenbottam, 1989). In general, a breathhold of 10 sec should not increase endogenous levels above 50-100 ppb; thus, we are interested in maintaining exhaled exogenous levels above 1 ppm (1000 ppb) to avoid contamination from endogenous production. To investigate the impact of lung volume on D_L in the prolonged breathhold maneuver, we had each subject repeat the maneuver at two different inspired volumes: (1) $\approx 50\%$ of vital capacity (VC); or (2) VC. To facilitate this maneuver, a pneumatic valve was placed at port 2 and was closed manually when the desired inspired volume was reached.

2.12. Data analysis

NO, CO, CH₄ concentration (C_{NO} , C_{CO} , C_{CH4}) and volume (V) were continuously recorded throughout the single breath and were stored in a computer. C_{NO} , C_{CO} , C_{CH4} were synchronized with V by aligning the start of inspiration in the signals while correcting for the rise times of the instruments, and taking into consideration the transport delay through $V_{DS,insp}$ (Fig. 2). The volume of the inspired gas was adjusted by subtracting $V_{DS,insp}$ and the anatomic dead space, $V_{DS,A}$ (assumed constant and equal to 150 ml) (ATS, 1987). The alveolar volume during exhalation (V_A) was also adjusted by adding $V_{DS,A}$ and $V_{DS,EXP}$.

The initial 750 ml of exhaled volume was discarded, which was sufficient to wash-out $V_{\rm DS,A}$

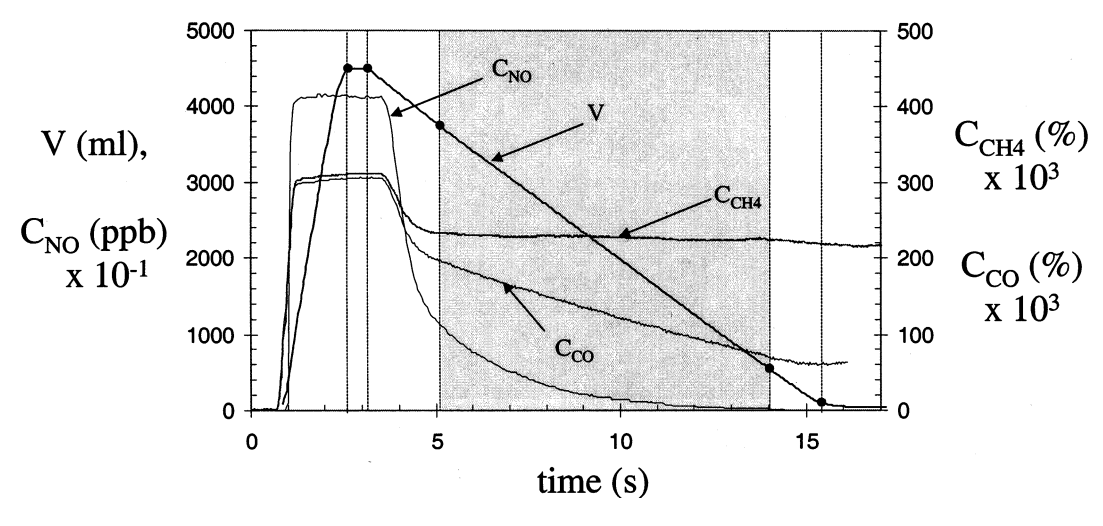


Fig. 2. Representative experimental data for a constant exhalation maneuver. Concentrations of tracer gases and volume are shown as a function of time for a typical constant exhalation maneuver. The solid circles on the volume curve represent the following in sequential order: (1) end of inspiration; (2) end of breathhold (≈ 0.5 sec); (3) end of deadspace washout and beginning of exhalation data for data analysis; (4) end of exhalation data for analysis, or closing volume; and (5) end-exhalation. The shaded region highlights the portion of the exhalation curves used in the data regression analysis.

and $V_{DS,exp}$. The remainder of the prolonged constant exhalation, up to closing volume, was used for the analysis (shaded area in Fig. 2). The residual volume, V_{RV} , was estimated by the dilution of the inert gas (CH₄). For this calculation, we used the exhaled CH₄ concentration just before the closing volume ($C_{E,CH4}(V_{CV})$).

For the prolonged breathhold maneuver, the standard Jones–Meade method was employed (Jones and Meade, 1961; ATS, 1987). An exhaled sample of 1 L immediately following the discarded volume was used for the analysis. The sample was not physically collected; however, the rapid response analyzers enabled us to estimate the concentration of CH₄, CO, NO for the sample by integrating the exhalation signals with respect to volume.

2.13. Statistics

All comparisons between different parameters are made using either a two-tailed paired or two-tailed unpaired Student t-test with significance at P < 0.05.

3. Results

As mentioned earlier, for the model analysis, the model equations (Eqs. (1) and (2)) are used to generate 'experimental' data (i.e. $C_E(t)^*$). In this manner, research conclusions for the suitability of the model to identify the unknown parameters are independent of the features of the specific experiment. Values for the baseline or control nominal

Table 1 Nominal parameter values for \tilde{X}_{o} and \tilde{Y}_{o}

Vector	V _{Ao} (L)	$\dot{V}_{I} \text{ (ml sec}^{-1}\text{)}$	t_{bh} (sec)	\dot{V}_{E} (ml/sec)	C _I (NO, CO) (ppm, %)	C _{I,CH4} (%)	а _{Е,СН4} (%)	b _{E,CH4} (%/L)
$ ilde{ ilde{X}_{ m o}}$	5.15	2000	0.5	350	40, 0.3	0.3	0.225	0.003
$ ilde{Y}_{ m o}$	a (ml/sec) 220	b (ml/(sec L)) 20	k_{CO} 0.5		α (ml/sec $L^{-\beta}$) 500	β 0.8	$k_{ m NO} \\ 0.5$	

points \tilde{X} o, \tilde{Y} o used in the simulations are given in Table 1.

3.1. Least squares minimization

The ability of the quasi Newton algorithm to minimize the SSE was tested in several different simulations. The model fitted the 'experimental' data satisfactorily (root mean square of residuals, RMSR = $\sqrt{\frac{\text{SSE}_a}{l}} < 10^{-4}\%$ CO or < 1ppb NO), and the identifying parameters agreed with the nominal values (relative error < 10^{-4}). In addition, the partial derivatives computed using the ADIFOR generated code were verified using a finite difference scheme in selective cases.

3.2. Sensitivity analysis

Fig. 3A and B investigate the sensitivity for CO and NO, at different nominal values (i.e. at different points in the (n+m)-dimensional space). From the infinite number of possible combinations of nominal parameter values, we decided to examine the effect of four parameters: V_{Ao} , \dot{V}_{I} , \dot{V}_{E} , and t_{bh} . These parameters have the greatest potential for variation in an experimental protocol, while the remaining parameters are usually kept constant. Thus, we seek to examine the sensitivity of the model over different potential experimental conditions to identify conditions of maximum sensitivity. We performed simulations for four different V_{Ao} (3.15, 4.15, 5.15, and 6.15 L), four different \dot{V}_{I} (0.5, 1.0, 2.0, and 3.0 L/sec), three different \dot{V}_{E} (0.35, 0.7, and 1.05 L/sec) and three different t_{bh} (0.5, 3, and 7 sec). Thus, $\hat{S}_{f,\tilde{Y}}(\tilde{X}_0,\tilde{Y}_0)$ was estimated at a total or 144 $(4 \times 4 \times 3 \times 3)$ different points for CO and NO. The sensitivity for the control nominal values is shown for comparison (point #11 with darker color). $\hat{S}_{f,a}$ increases with V_{Ao} , while it decreases when $\dot{\mathbf{V}}_{\mathbf{I}}$ or $\dot{\mathbf{V}}_{\mathbf{E}}$ is increased. $\hat{S}_{f,b}$ also increases

with V_{Ao} , while $\hat{\bar{S}}_{f,\,k}$ is mostly affected by \dot{V}_{I} in an inverse fashion. For NO (Fig. 3B), $\hat{\bar{S}}_{f,\,\alpha}$ increases with both \dot{V}_{I} and \dot{V}_{E} . $\hat{\bar{S}}_{f,\,\beta}$ depends mostly on V_{Ao} in a positive fashion and $\hat{\bar{S}}_{f,\,k}$ decreases with \dot{V}_{I} .

In addition the sensitivity of the estimated parameters with respect to the experimentally measured ones (\tilde{X}) was investigated, under different experimental conditions (Tsoukias, 1999). Parameters a and b are most sensitive to error in V_{Ao} . Estimation of k_{CO} is affected significantly by the value of C_{I} , $C_{I,CH4}$ and $a_{E,CH4}$. α and β are not very sensitive to errors in the experimentally measured parameters. Estimation of k_{NO} will be sensitive to the values of C_{I} , $C_{I,CH4}$ and $a_{E,CH4}$, and to a lesser extent to the values of t_{bh} and \dot{V}_{E} (Tsoukias, 1999).

3.3. Identifiability analysis

Fig. 4A presents the root mean squares of residuals $\left(\sqrt{\frac{\text{SSE}_a}{l}}\right)$ for CO using different combinations of values for a and b and optimal k_{CO} (i.e. $\min_{k} \{ SSE_a(a, b, k_{CO}) \}$). Fig. 4B presents different combinations of a and $k_{\rm CO}$ for optimal b. The graphs are repeated for NO in Fig. 5A and B. All the simulations are performed using the control nominal parameter values. The first observation is the absence of multiple global minimum points, at least in the range of parameter values examined. Thus, a global unidentifiability problem does not exist for either case. However, there exist multiple combinations of a and b that produce essentially the same very small SSE_a, suggesting a dependence (or local unidentifiability) between these two parameters (more accurately 'ill conditioning'). The combinations of a and b that effectively 'minimize' the SSE form a line of multiple 'minimum' points that includes the point of the nominal parameter values (a = 220 ml/sec, b = 20ml/sec/L) (true minimum or $SSE_{\alpha} = 0$). Thus, for an arbitrary value for a, relatively close to the

Fig. 3. The time-averaged (root mean square) semi-relative sensitivity function, $\hat{S}_{f,\tilde{Y}}(\tilde{X}_{o},\tilde{Y}_{o})$, is shown for 144 different experimental conditions (or 144 different values of \tilde{X}_{o}) for CO (A) and NO (B). Four different V_{Ao} (3.15, 4.15, 5.15, and 6.15 L), four different \dot{V}_{I} (0.5, 1.0, 2.0, and 3.0 L/sec), three different \dot{V}_{E} (0.35, 0.7 and 1.05 L/sec) and three different t_{bh} (0.5, 3, and 7 sec) were used in the simulations. The sensitivity for the control nominal values is shown for comparison (11th point, shown with darker color and larger circle).

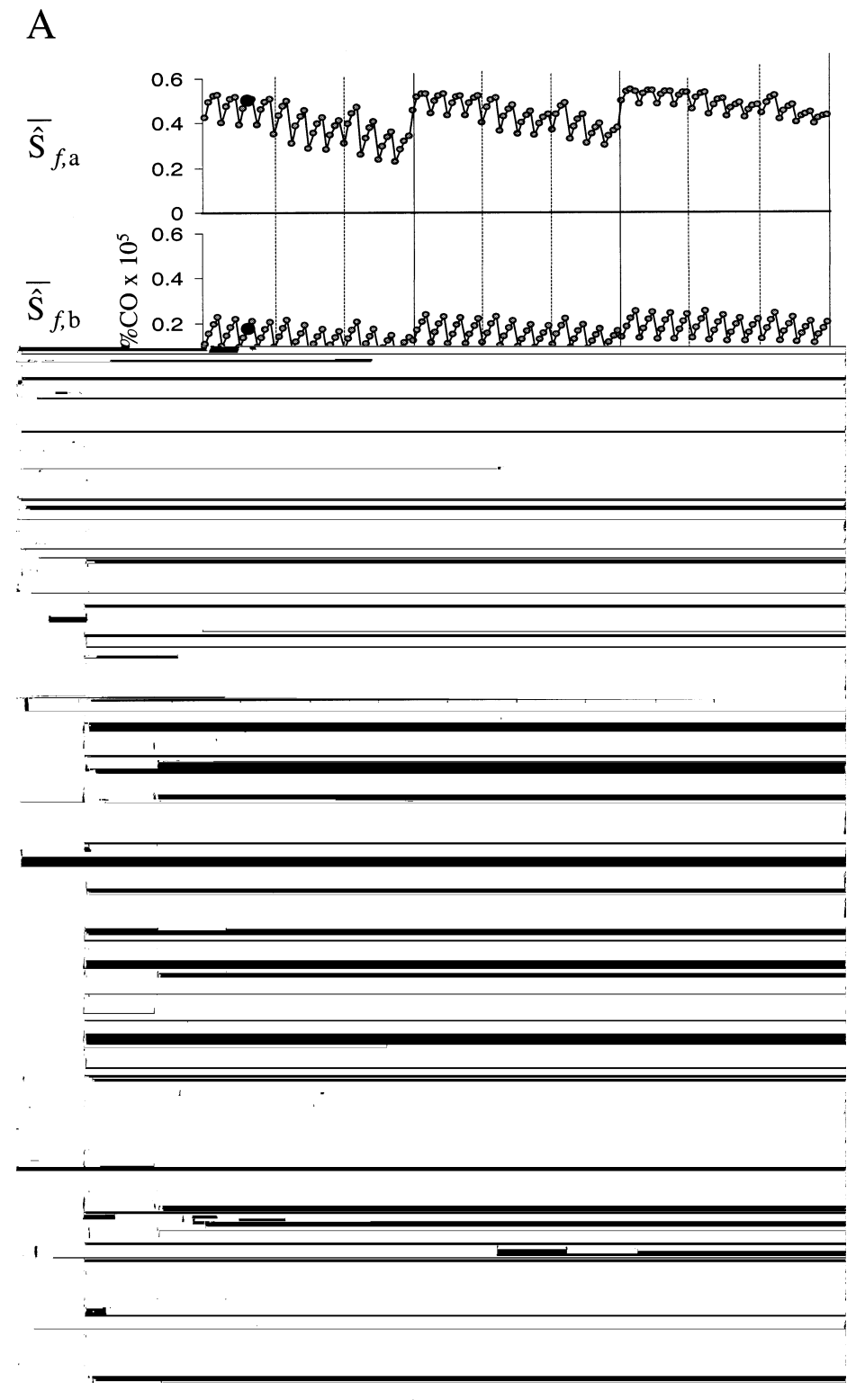


Fig. 3.

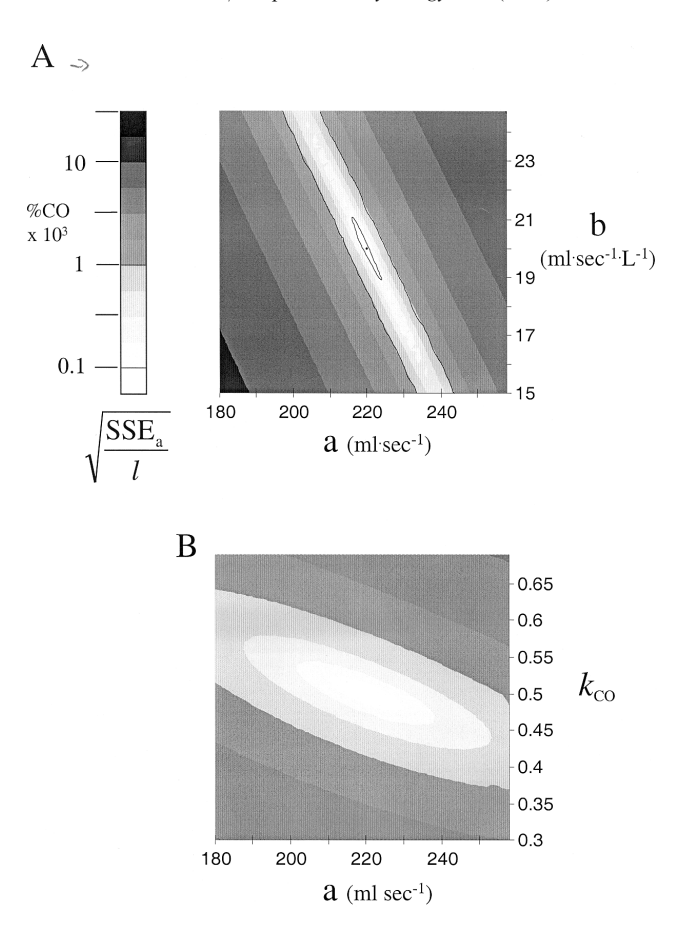


Fig. 4. RMSR is shown for CO using different combinations of values for a and b, and then finding the optimal k (A), and then different combinations of a and k following determination of optimal b (B). All the simulations were performed using the control nominal parameter values. The gray scale bar represents values for RMSR and is shown for reference.

nominal value, there will be a small range of values for b that produces a satisfactory fit to the experimental data.

In Fig. 4B a similar line is formed; however, the line is essentially horizontal and much shorter (spanning a small range of k's) suggesting that for any given a and optimal b the optimal $k_{\rm CO}$ will have essentially a single and identifiable value. Thus, there is no dependence between $k_{\rm CO}$ and a. Furthermore, since for any optimal set of a and b the value of $k_{\rm CO}$ will be essentially constant, $k_{\rm CO}$ will be independent of b as well (thus, the corresponding $b-k_{\rm CO}$ diagram is not shown).

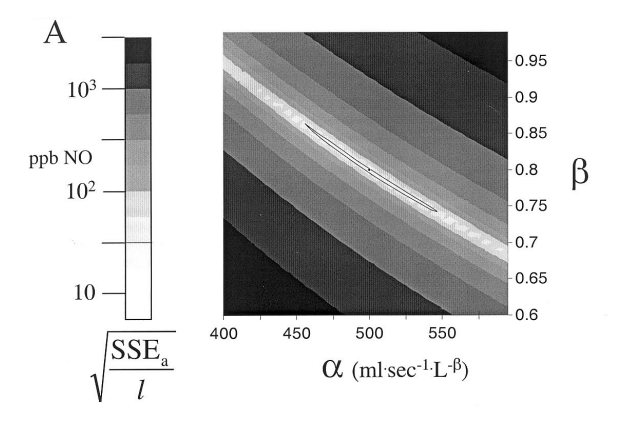
The same phenomenon appears in Fig. 5A and B for NO. There is a dependence between α and β resulting in multiple points (combinations of α

and β) along a single line, that accurately fits the data (Fig. 5A). This slightly curvilinear relationship includes the point of the nominal parameter values ($\alpha = 500 \text{ ml/sec/L}^{-8}$, $\beta = 0.8$) where SSE_a is exactly zero. In all of these points, the value of $k_{\rm NO}$ will remain essentially constant (Fig. 5B), suggesting that $k_{\rm NO}$ can be uniquely identified.

In Fig. 4A, the dependence of b on a is approximately linear (i.e. b = s*a + p). The coefficients s and p, estimated with linear regression, are -0.265 and 78.2, respectively. The slightly curvilinear dependence of β on α in Fig. 5A is described accurately via a logarithmic dependence (i.e. $\beta = q*\ln(\alpha) + r$). The coefficients q and r are estimated with regression as -0.669 and 4.46, respectively. The procedure can be repeated for

determining the optimal sets of parameters that minimize the SSE_r for both cases. This results in slightly different curves (data not shown) that intersect at a common point which is equal to the point of the nominal control values for a and b, or α and β (that is, the true minimum, or $SEE_a = 0$ and $SSE_r = 0$). Thus, utilizing weighted least squares methods (chi-squared value) might improve the estimation of the optimal combination of a and b, or α and β .

In Fig. 6 we plot the functional dependence of D_{LCO} (Fig. 6A) and D_{LNO} (Fig. 6B) on V_A . The set of nominal values of a and b (or α and β) was used (thick lines) as well as different optimal sets of a and b (or α and β) (thin lines). The plots reveal that for both CO and NO, the different



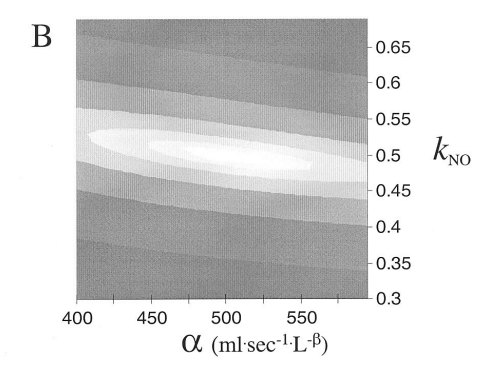
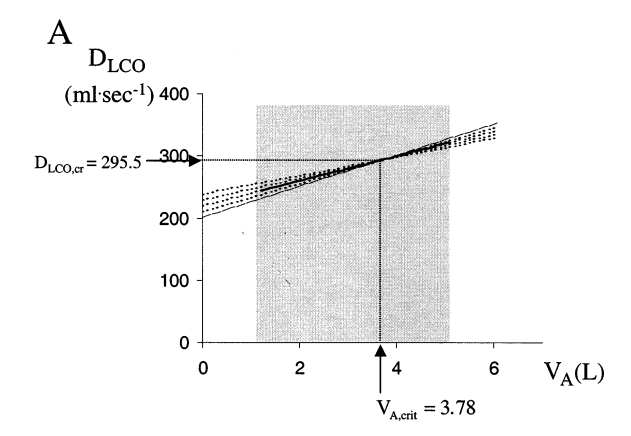


Fig. 5. RMSR is shown for NO using different combinations of values for α and β , and then finding the optimal k (A), and then different combinations of α and k following determination of optimal b (B). All the simulations were performed using the control nominal parameter values. The gray scale bar represents values for RMSR and is shown for reference.



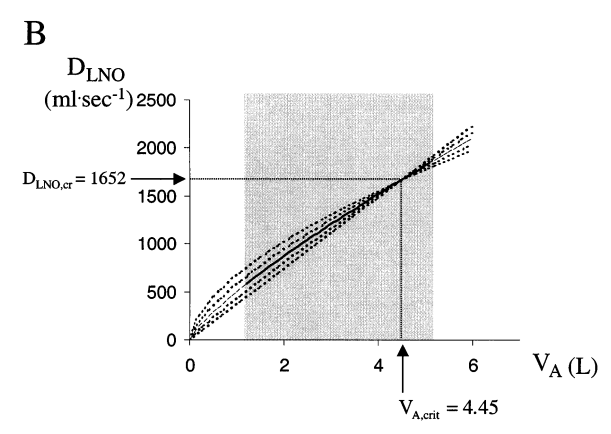


Fig. 6. Functional dependence of $D_{\rm LCO}$ (A) and $D_{\rm LNO}$ (B) on $V_{\rm A}$. The set of nominal values of a, b (or α and β) are used (thick lines) as well as different optimal sets of a and b (or α and β) (thin lines). The largest deviations represent a 25% variation in b or β from the nominal control value.

optimal sets of a and b (or α and β) represent a family of curves for the functional dependence of $D_{\rm L}$ on $V_{\rm A}$ with a single point that is common to all of the curves. This common or critical point ($V_{\rm A,cr}$, $D_{\rm L,cr}$) can be predicted from the coefficients s and p (or q and r) (proof not shown (Tsoukias, 1999)). For the control nominal parameter values, $D_{\rm L,cr}=296$ ml/sec for CO at $V_{\rm A,cr}=3.78$ L, and a $D_{\rm L,cr}=1650$ ml/sec at $V_{\rm A,cr}=4.45$ L for NO. Thus, although the dependence between a and b (or α and β) does not allow one to characterize the functional dependence between $D_{\rm L}$ and $V_{\rm A}$ with zero uncertainty, one can uniquely identify $D_{\rm L}$ ($D_{\rm L,cr}$) at a specific $V_{\rm A}$ ($V_{\rm A,cr}$) that lies in the middle region of the examined alveolar volumes

 $(V_{Ao} - V_{RV})$. The error in the estimate of D_L progressively increases as V_A deviates from $V_{A,cr}$ (Fig. 6).

The functional dependence of α on β (and to a lesser extend of a on b) is slightly different when SSE_r is used in the minimization. When the relative error is used, the later part of the profile (lower concentrations) is predicted better than the early part when compared to using the absolute error. As a result, the critical point appears later (smaller V_{A.cr}) generating a different dependence between a and b, and α and β . The difference between relative and absolute minimization is more profound for NO where the concentration decreases rapidly over a larger range of concentrations than CO. In general, a weighted least squares method (χ^2 -minimization) that accounts for variation in the measured output at each point is optimal, but requires knowledge of the variance of the measurement error (Chatterjee and Price, 1977). However, this detailed information depends heavily on the specific experimental set-up and analytical instrument and is not always available.

Thus, the minimization algorithm provides:

$$\{a, b, k_{\text{CO}}\} = \{(D_{\text{L,cr}} - b \ \text{V}_{\text{A,cr}}), b, k_{\text{CO}}\}$$
where $(b_{\text{o}} - \Delta b) < b < (b_{\text{o}} + \Delta b)$ (12)
$$\{\alpha, \beta, k_{\text{NO}}\} = \left\{ \left(\frac{D_{\text{L,cr}}}{(\text{V}_{\text{A,cr}})^{\beta}}\right), \beta, k_{\text{NO}}\right\}$$
where $(\beta_{\text{o}} - \Delta \beta) < \beta < (\beta_{\text{o}} + \Delta \beta)$ (13)

where the value b or β lies somewhere in a range around the nominal or 'true' value b_o or β_o . The confidence region for b (or β) will depend on the accuracy of the least square fit (i.e. sum of squares of error) and can be estimated utilizing the F-statistic test as described in Eq. (11). Thus, a more appropriate description for the estimated D_L is:

$$D_{\rm LCO} = D_{\rm L,\,cr} + b({\rm V_A - V_{A,\,cr}}), \quad b = b_{\rm o} \pm \Delta b \eqno(14)$$

$$D_{\rm LNO} = D_{\rm L, cr} \left(\frac{V_{\rm A}}{V_{\rm A, cr}} \right)^{\beta}, \quad \beta = \beta_{\rm o} + \Delta \beta$$
 (15)

Parameters a and α have been replaced by their functional linear and logarithmic dependence on b or β , respectively. Thus, $D_{\rm L}({\rm V_A})$ is represented as

a function of three unknown parameters that need to be identified (i.e. $D_{\rm L,cr}$, $V_{\rm A,cr}$, and b or β). $D_{\rm L,cr}$ and $V_{\rm A,cr}$ can be accurately estimated for each maneuver utilizing multiple minimizations (i.e. find a series 'optimal' combinations of a and b, or α and β). Only parameter b or β will then vary (by Δb or $\Delta \beta$) around the true or nominal value $b_{\rm o}$ and $\beta_{\rm o}$.

The above relationships indicate that a very accurate estimate for $D_{\rm L}$ at a specific point ($V_{\rm A,cr}$) can be obtained, but the uncertainty increases as $V_{\rm A}$ diverges from $V_{\rm A,cr}$. In order to reduce this uncertainty, the best possible estimation for b (or β) is sought. Thus, for the experimental data, parameter b or β is estimated as an average of the optimal points from multiple maneuvers utilizing minimization of the absolute and relative error.

3.4. Experimental data

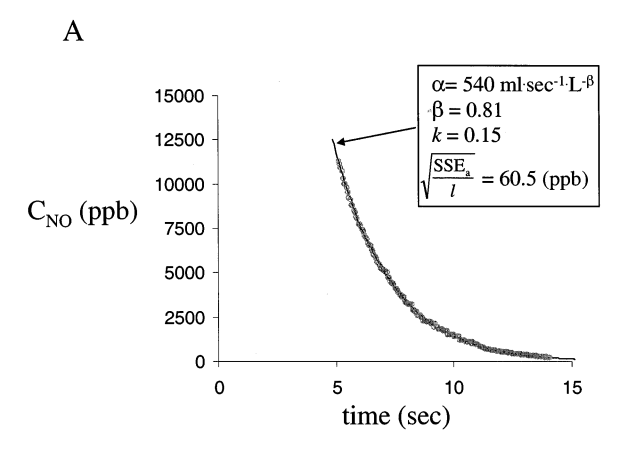
The above theoretical considerations were applied in the analysis of the data collected from the human subjects. Although D_L was measured in ml/sec (ATPS) (C_E is measured in ATPS) we converted our result to the more standard units of ml/min/mmHg (STPD). Fig. 7A presents the least square fit of the experimental NO data of the representative example in Fig. 2. The root mean square of residuals (RMSR) between the experimental data and our simulation was 60.5 ppb. Employing multiple minimization for the sum of squares of the absolute error (SSE_a) (i.e. for different α 's near the optimal value we identify the optimal set of β and k) multiple combinations of α and β are identified that can satisfactory fit the experimental data (Fig. 7B). The same procedure was repeated for CO to identify optimal parameter combinations for a and b. Typical values for RMSR in the CO simulations were 10^{-30} % CO (data not shown).

Figs. 8 and 9 plots the results for $D_{\rm LCO}$ and $D_{\rm LNO}$ for all constant exhalation maneuvers and for all seven subjects. The point of maximum confidence for $D_{\rm L}$ (V_{A,cr}, $D_{\rm L,cr}$) is indicated with a star (*), and represents an average value in all maneuvers performed by the subject. At this average V_{A,cr} the variation in $D_{\rm L}$ between maneuvers is minimal (<2%). Dotted lines represent the

dependence of $D_{\rm LCO}$ ($D_{\rm LNO}$) on ${\rm V_A}$ in the presence of NO, while solid lines in Figs. 8 and 9 are from the control experiments. The thick line represents the $D_{\rm L}$ prediction for the average value of b or β from all maneuvers performed by the subject. The shaded area indicates the part of the exhaled profile (${\rm V_A}$) used in the regression analysis. A limited number of maneuvers were discarded if the exhaled volume for analysis was < 1.5 L, or if the values for b or b were greater or less than two standard deviations from the mean. The Jones–Meade estimations of $D_{\rm LCO}$ and $D_{\rm LNO}$ from the

prolonged breathhold maneuvers are also presented in Figs. 8 and 9 for comparison (solid circles), and are plotted at V_{Ao} (i.e. the alveolar volume during breathholding where most of the gas exchange occurs). The majority of the measurements made using the Jones–Meade technique are smaller than the estimate used with our model, and this finding is statistically significant (P < 0.01).

Table 2 compares estimated $D_{\rm LCO}$ in the presence and absence of NO in the test gas. Since $D_{\rm LCO}$ depends on $V_{\rm A}$ (Eq. (14)), the comparison is



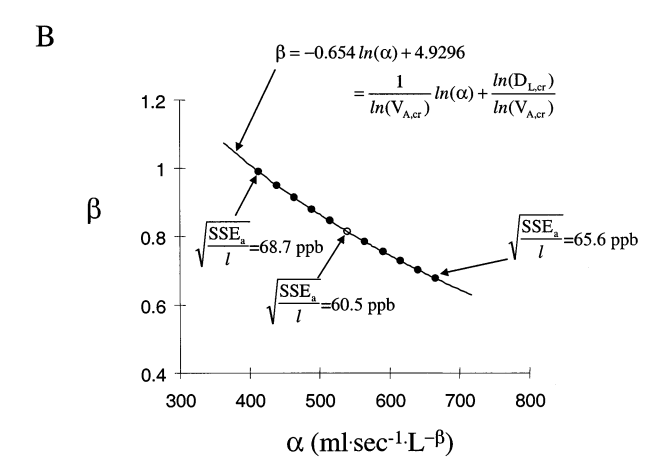


Fig. 7. Regression analysis of representative data for NO shown in Fig. 2 (A). The average difference between the experimental data and our simulation was 60.5 ppb, and values for the remaining regression parameters are shown. Regression analysis using the absolute error (SSE_a) is shown for the experimental data in Fig. 6 beginning with different α 's near the optimal value (α = 42.6) and determining the corresponding optimal β and k (B). Multiple combinations of α and β produce a similar average error (range 60.5–68.7 ppb). The solid line represents a logarithmic regression of the dependence between α and β . Note that the logarithmic regression parameters are used to determine $D_{L,cr}$ and $V_{A,cr}$.

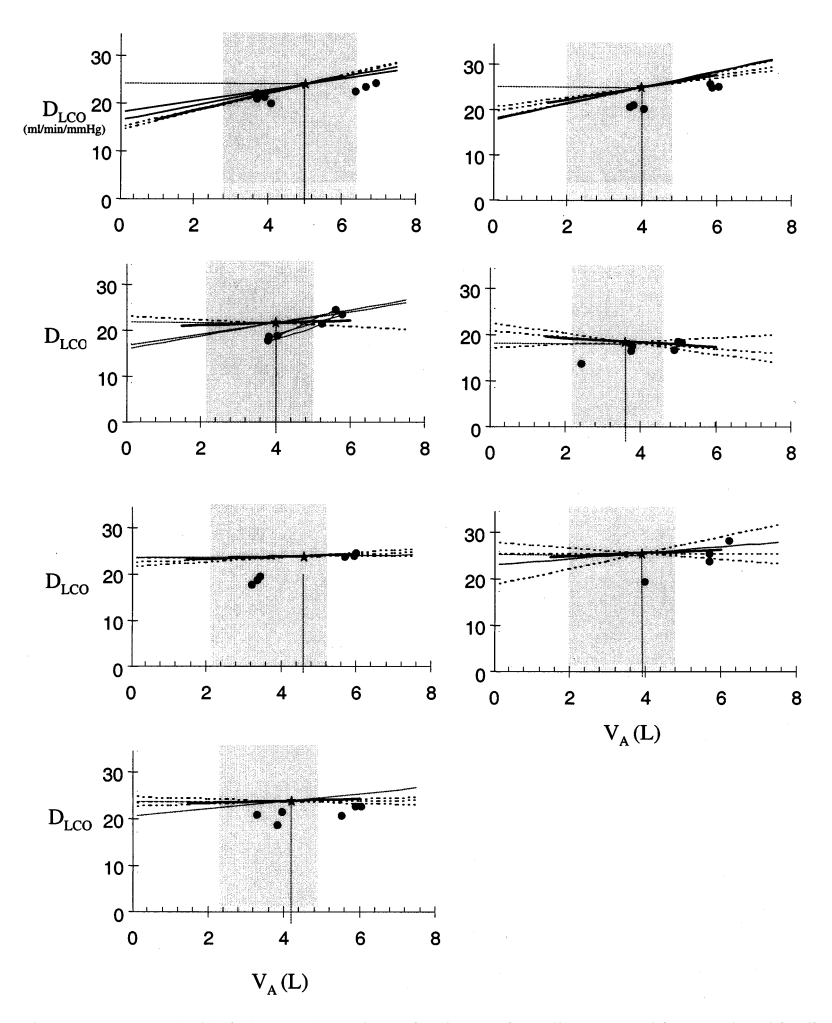


Fig. 8. The dependence between $D_{\rm LCO}$ (ml/min/mmHg) and $V_{\rm A}$ is shown for all seven subjects. The thin lines (dashed is in the absence of NO, solid in the presence of NO) represent the model prediction using the values for a, b, and $k_{\rm CO}$ from the regression analysis for each maneuver. The thick line is the model prediction using the mean values for a, b, and $k_{\rm CO}$ from the regression analysis of all of the maneuvers. The shaded region represents the minimum alveolar volume for which the data was attained. The star indicates $D_{\rm L,cr}$ and $V_{\rm A,cr}$, and the solid circles are $D_{\rm LCO}$ determined from a breathhold maneuver and determined from the Jones–Meade method.

made at $V_{A,cr}$. Since small variations of $V_{A,cr}$ exists between maneuvers, D_{LCO} was estimated at the average value of $V_{A,cr}$ according to Eq. (14). In the presence of NO, the average value of D_{LCO} in six of the seven subjects is slightly higher; however, this difference is not statistically significant (P > 0.05).

Estimates for b and β for each subject are summarized in Fig. 10A and B (i.e. average values in all maneuvers performed by the subject (\pm

S.D.)). For six of the seven subjects, $D_{\rm LCO}$ increases with $V_{\rm A}$ (Fig. 8 or Fig. 10A). The average value (\pm S.D.) for b in all seven subjects is 0.69 (\pm 0.79), which is statistically different from zero (P < 0.05) indicating that $D_{\rm LCO}$ is not constant. The variation of β between maneuvers within the same subject is small (Fig. 9 or Fig. 11B). This provides highly reproducible estimates for $D_{\rm LNO}$, especially within the examined part of $V_{\rm A}$ (shaded area of Fig. 9). The average value (\pm S.D.) of β

for all subjects is 0.65 (\pm 0.19), which corresponds to the lower limit (i.e. 2/3) of the predicted range for β according to a simple model for the membrane diffusing capacity (Tsoukias et al., 2000). In addition, the average β is statistically less than one (i.e. dependence of $D_{\rm LNO}$ on $V_{\rm A}$ is not linear) and statistically larger than zero (i.e. $D_{\rm LNO}$ is not constant). Based on the above values and the average values for $D_{\rm LCO}$ and $D_{\rm LNO}$ at $V_{\rm A,cr}$ the following average relationships were es-

tablished: $D_{LCO} = 20 + 0.7 \cdot V_A$ and $D_{LNO} = 48 \cdot V_A^{2/3}$ ml/min/mmHg (STPD) where V_A is expressed in L (STPD).

Fig. 11 presents estimated values for k, estimated either from the exhaled CO data ($k_{\rm CO}$) or the exhaled NO data ($k_{\rm NO}$). The average value (\pm S.D.) for $k_{\rm CO}$ in all seven subjects was 0.56 (\pm 0.30) and is slightly higher than $k_{\rm NO}$, 0.46 (\pm 0.40). However, this difference is not statistically different from zero (P < 0.05). In addition,

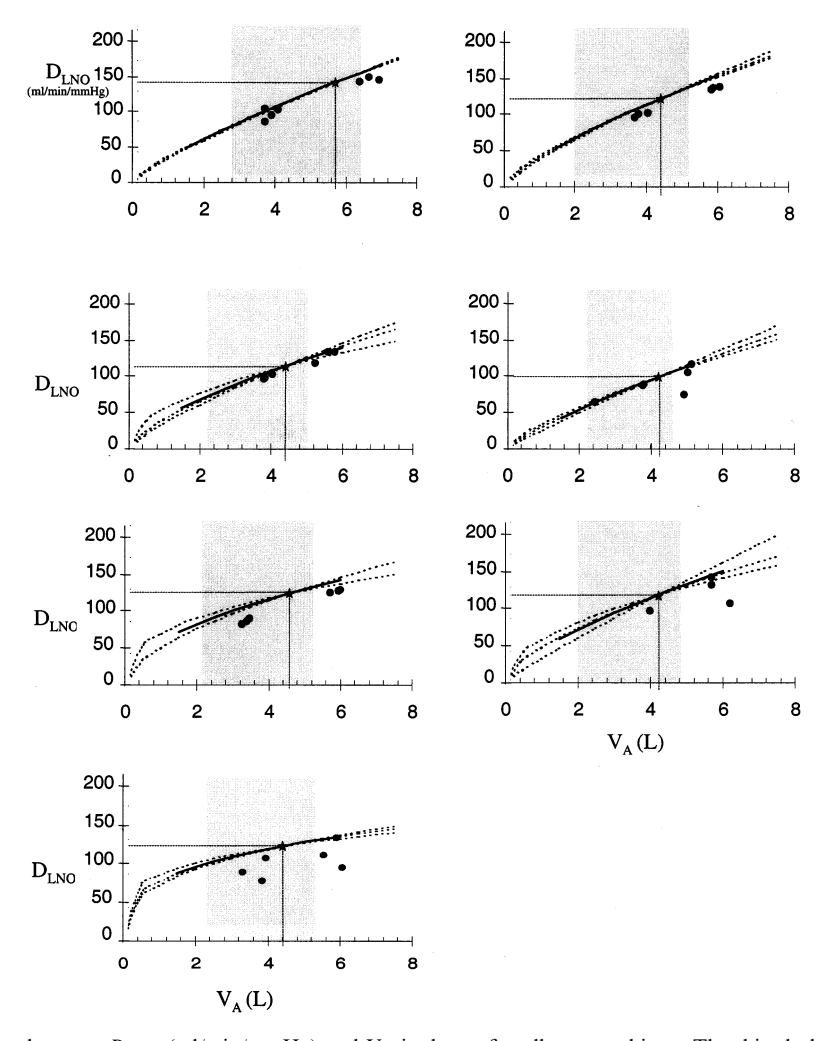


Fig. 9. The dependence between $D_{\rm LNO}$ (ml/min/mmHg) and $V_{\rm A}$ is shown for all seven subjects. The thin dashed lines represent the model prediction using the values for α , β , $K_{\rm NO}$ from the regression analysis for each maneuver. The thick line is the model prediction using the mean values for α , β , and $K_{\rm NO}$ from the regression analysis of all of the maneuvers. The shaded region represents the minimum alveolar volume for which the data was attained. The star indicates $D_{\rm L,cr}$ and $V_{\rm A,cr}$, and the solid circles are $D_{\rm LNO}$ determined from a breathhold maneuver and determined from the Jones-Meade method.

Table 2 D_{LCO} in the presence or absence of NO

Subject	$V_{A,cr}(L)$	$D_{\rm LCO}$ (ml/min/mmHg)			
		NO present	NO absent		
1	5.03	25.1	22.6		
2	4.11	24.8	25.4		
3	4.00	21.9	21.5		
4	3.61	19.3	17.4		
5	4.34	24.2	23.3		
6	3.92	25.7	25.1		
7	4.08	24.0	23.4		
Average (S.D.)		23.6 (2.2)	22.7 (2.7)		

both k_{CO} and k_{NO} are statistically different from 0 and 1, the limits of a well-mixed and a se-

quentially filled unmixed alveolar region, respectively.

4. Discussion

4.1. Sensitivity analysis

In exploring the suitability of the model for parameter identification we first examine the sensitivity of the identifying parameters on the model's output. A small sensitivity suggests that an unacceptable large range of values for the respective parameter can satisfactorily represent the data, posing a problem for the identification. Thus, sensitivity analysis can provide a first description for the expected variation in the estimated parameters, relative to the error in the

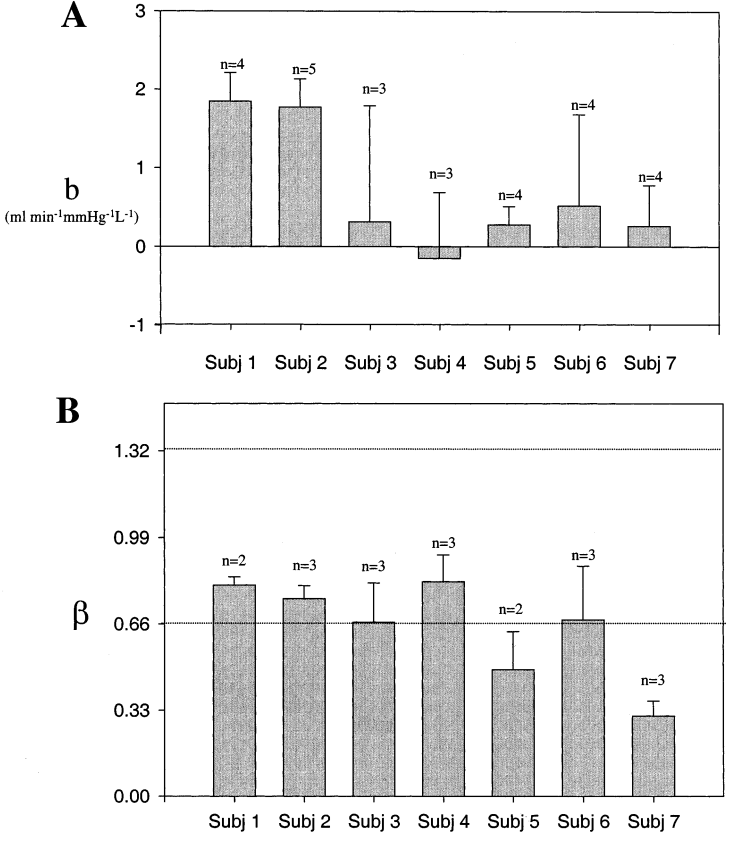


Fig. 10. Estimates for b (A) and β (B) from regression analysis for each subject are summarized. The bar represents the average values in all maneuvers performed by the subject (\pm S.D.) with the number of maneuvers shown in parentheses. Two values of β are highlighted (2/3 and 4/3) for reference, which represent theoretical limiting cases.

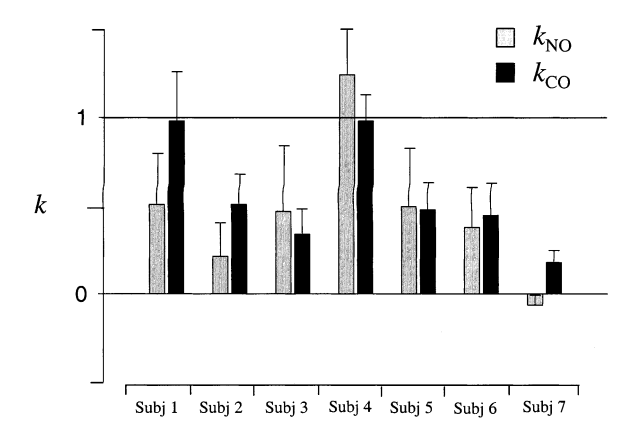


Fig. 11. Estimates for k using the regression from CO (kCO) and NO (kNO) for each subject are summarized. The bar represents the average values in all maneuvers performed by the subject (\pm S.D.). Note that a value of k=1 represents the limit of a completely sequentially filled alveolar region, and k=0 represents complete alveolar mixing.

measurement in C_E or the accuracy of the least square fit. Thus, one can use $\bar{\hat{S}}_{f,\;\tilde{\gamma}}$ to predict the required accuracy for the experimental measurement of the model's output needed to provide an estimate for the identifying parameter within an acceptable range.

Fig. 3A and B reveal that optimal sensitivity for each unknown parameter is not accomplished under the same conditions; however, several general conclusions can be made. In the examined range of experimental conditions, analysis of CO data is improved at high V_{Ao}. If V_{Ao} is large, then one should also employ low \dot{V}_E and \dot{V}_I . For NO, one should employ high \dot{V}_E . \dot{V}_I should be kept high if one is interested in estimating α or β , but low if high accuracy on k is desirable. A small breathhold time (≈ 0.5 sec) is most appropriate for both gases. If estimation of all of the unknown parameters is equally important then criteria for optimal experimental conditions can be formed by examining the covariance matrix of the estimator vector \tilde{Y} (Badavas and Saridis, 1970; Beck and Arnold, 1977). The above analysis suggests experimental conditions that improve sensitivity. However, the unknown parameters might depend on these conditions (i.e. \dot{V}_{I} may affect the distribution of ventilation and thus k). Thus, caution is advised in choosing experimental conditions, and

the choice should not be performed based solely on the above criteria.

 $\hat{S}_{f, \ \bar{\gamma}}$ at the control nominal values (solid circle in Fig. 3A and B) were approximately 0.5, 0.2 and 0.1 × 10⁻³% CO per % change in a, b or k, respectively, and 75, 95 and 20 ppb per percent change in α , β or k, respectively. The above values can be interpreted as the root mean square error induced in the model output from a 1% perturbation of the unknown parameter. Thus, sensitivity analysis suggests that a necessary condition for the estimation of a, b and k (or α , β and k) to be within 1% is the following: the standard error in the measurement of C_E should be at least three orders of magnitude less than the inspired concentration (i.e. instrument error of 0.1 × 10⁻³% CO or 20 ppb NO).

4.2. Identifiability analysis

The two-dimensional images in Figs. 4 and 5 reveal a dependence between parameters a and b (or α and β) and thus, a local unidentifiability problem (ill-conditioning). The variation of the predicted parameters will be directly related to the accuracy of the experimental measurement and the ability of the model to simulate the data. Fig. 4A and Fig. 5A provide an estimation of the expected variation in a and b (or α and β) for a given level of accuracy in the fitting of the data (confidence region). Values for b in a range +5%from the nominal value can predict the experimental exhalation profile with a RMSR less than 0.1×10^{-3} % CO. For RMSR less than $0.2 \times$ 10^{-30} % CO, the range of uncertainty in b increases to 20%. For NO, values for β in a range \pm 10% from the nominal value can predict the data with a RMSR less than 30 ppb. For an RMSR less than 95 ppb the range increases to 25%.

Comparing the results above with those from the sensitivity analysis, it is evident that the local unidentifiability problem between a and b, and α and β poses the more serious threat for suitability of the model for parameter identification. At a confidence region described by the contour with RMSR of $0.2 \times 10^{-30}\%$ CO or 95 ppb NO, the uncertainty in the estimate for b or β increases

from 1% to 20 and 25%, respectively. Eq. (11) relates the confidence region to the minimum SSE. When the SSE approaches zero the confidence region is minimal and parameters can be accurately estimated. At a confidence level of 95%, the confidence region includes all combinations of the unknown parameters that meet the following criteria: RMSR(\tilde{Y}) < 1.041*RMSR-(\tilde{Y}_f)($F_{1-0.05}(3.97) = 2.7$).

In an effort to improve the ability of the model to identify the parameters, we explored the nature of the dependence between the parameters. The functional dependence of a and b (or α and β) can be best described by a linear (or logarithmic) relationship. The different optimal combinations of a and b (or α and β) describe different curves for the dependence of D_L with V_A , which all intersect at a single point (Fig. 6). Thus, although the multiple 'optimal' combinations of parameters does not allow one to uniquely determine $D_{\rm I}(V_{\rm A})$ over the entire range of VA, one can achieve an excellent prediction for $D_{\rm L}$ at a single specific $V_{\rm A}$. This critical point of minimum uncertainty for $D_{\rm L}$, (denoted $D_{\rm L,cr}(V_{\rm A,cr})$) will be independent of the 'optimal' combination of a and b (or α and β), and will be subject and maneuver specific. Such a result is, perhaps, anticipated based on the fact that the uncertainty in estimating D_L should increase as V_A diverges either direction from the range of V_A used in the regression analysis. Thus, a single V_A, somewhere in the middle of the V_A used in the regression analysis, should result that has the minimum uncertainty in $D_{\rm L}$.

Estimation of $D_{\rm LCO}$ is unaffected by the presence or absence of NO. Although there is a small increase on the average $D_{\rm LCO}$ (Table 2) in the presence of NO (perhaps due to pulmonary vasodilation and increase in pulmonary capillary volume), this difference is not statistically significant. This finding is consistent with the study of (Borland and Higenbottam, 1989) who utilized the Jones–Meade method to determine the simultaneous measurement of $D_{\rm LCO}$ and $D_{\rm LNO}$.

Fig. 7A demonstrates that the model can predict the experimental data quite accurately. A portion ($\approx 40\%$) of the root mean square error (60.5 ppb for NO) can be attributed to the inherent noise of the signal (i.e. smoothing the data

with a moving average reduces the average error to a minimum of 37 ppb). The remaining error can be attributed to the quality of the maneuver performed by the subject (i.e. variation in the flow rates), the accuracy of the experimental measurements, and to other explicit model simplifications such as a homogeneous $D_{\rm L}$. The prediction of the data for CO is comparable to that of NO.

4.3. Diffusing capacity

Both $D_{\rm LNO}$ and $D_{\rm LCO}$ are best estimated within the alveolar volumes examined. The reproducibility of the measurement at $V_{\rm A,cr}$ for each subject was, on the average, less than 2% for both CO and NO. The average (mean \pm SD) value for b was statistically greater than zero (0.67 \pm 0.79 ml/min/mmHg/L) suggesting a slightly positive dependence on $V_{\rm A}$. This result is again in agreement with (Borland and Higenbottam, 1989) who reported an 8% decrease (38.5–35.5 ml/min/mmHg) in $D_{\rm LCO}$ when $V_{\rm A}$ changes from 7 to 3.9 L. One can then easily estimate a value for b of 0.97 ml/min/mmHg/L from their data, which although larger than our estimate (0.67), is certainly comparable.

The average (mean + SD) value of β was approximately 2/3 (0.65 \pm 0.19) which represents the lower range of expected values based on the simplified model of the membrane diffusing capacity for NO, D_{MNO} (Tsoukias et al., 2000). In addition, the mean value for β is statistically smaller than the upper limit of 4/3. A value of 2/3 is expected if either (but not both) of the following assumptions are valid: (1) the alveolar surface area available for diffusion remains constant during breathing, and only the membrane thickness changes (Staub, 1969); or (2) the change of $D_{\rm L}$ during breathing is attributed to unfolding of alveolar septa (increased alveolar surface area) and not to changes of membrane thickness (Weibel et al., 1973).

The inter- and intra-subject variation in the estimated value of b is larger than the variation in the estimate of β . This finding may be attributed to the local unidentifiability problem of b and β , with respect to the accuracy of the simulation of the exhaled profile for CO. RMSR of the model

prediction to the experimental data was approximately $10^{-3}\%$ CO while for NO was 60 ppb. Based on these values and according to Eq. (11) and Fig. 4 and Fig. 5, the expected variation on b and β should be > 25 and 15%, respectively. The sensitivity analysis revealed that this variation occurs mainly due to dependence between a and b (or α and β) and can be reduced with more accurate measurements of $C_{\rm E}$. In addition, estimation of b is particularly sensitive on $V_{\rm Ao}$; thus, part of the increased variation of b may be attributed to error in estimating $V_{\rm Ao}$ (Tsoukias, 1999).

4.4. Comparison with Jones-Meade

The Jones-Meade method underestimates both $D_{\rm LCO}$ and $D_{\rm LNO}$ (11 ± 8% and 12 ± 5% less for CO and NO, respectively). This finding is consistent with the model prediction in the companion manuscript (Tsoukias et al., 2000), and can be attributed to the following reasons. First, the Jones-Meade Method assumes a completely wellmixed alveolar compartment (k = 0), and thus neglects an additional effective alveolar concentration gradient due to sequential filling of the lung during inspiration. The experimental data suggest that the lung is filled, in part, sequentially (mean k = 0.51). Thus, the initial volume of gas exhaled has a shorter residence time in the alveolar region, and thus a larger concentration of test gas. A larger concentration of test gas causes the Jones-Meade method to underestimate $D_{\rm I}$. Second, the Jones-Meade method does not consider $D_{\rm I}$ as a positive function of $V_{\rm A}$. Thus, during inspiration, D_L of the lung is less than at the breathholding volume (V_{Ao}), the volume associated with the measurement technique, causing the method to underestimate $D_{\rm L}$.

The estimation of $D_{\rm L}$ using the new mathematical model is more reproducible than the Jones–Meade Method, especially at alveolar volumes near $V_{\rm A,cr}$. In addition, the new model and the single exhalation technique can derive information not only for $D_{\rm L}$ at a single volume, but can also determine the dependence of $D_{\rm L}$ with $V_{\rm A}$ through the parameters b and β . Similar information utilizing the Jones–Meade Method requires

multiple breathing maneuvers at different volumes. Even then only a small range of V_A can be examined since sufficient inspired volume is necessary for the test; thus, the dependence of D_L on small V_A cannot be explored. This is of critical importance for subjects or patients with reduced lung volumes such as those with chronic obstructive pulmonary disease (COPD).

4.5. Sequential filling

Values for k using exhaled data from either gas are in close agreement. The average k using both gases is 0.51, and is statistically different from both 0 and 1. This suggests that the alveolar region cannot be considered well-mixed or sequentially filled, and is not a surprising result (Dollfuss et al., 1967; Cotton et al., 1979). Importantly, a value for k that is different from zero has a substantial impact on the estimation of $D_{\rm L}$ (Tsoukias et al., 2000). The intra-subject variation in the estimate of k is significant, and is likely due to error in the experimental measurement of parameters such as inspired concentrations of the marker gas (i.e. NO) and inert gas (i.e. CH₄) (Tsoukias, 1999). The single parameter k represents an analytical technique to determine the degree of mixing or sequential filling during inflation of the lung. Our data suggest a value of 0.51 in normal lungs, but this may vary considerably in disease states such as COPD or bronchial asthma in which the filling pattern of the lungs is altered.

4.6. Implications for endogenous NO

Part of the motivation for developing the new mathematical model and its validation with experimental data is the relatively recent interest in understanding endogenous NO exchange. Endogenous NO is elevated in several inflammatory lung diseases, such as bronchial asthma; hence, there is interest in understanding the exhalation profile and a possible correlation with lung disease (Kharitonov et al., 1997). Certainly diffusion of endogenous NO into the pulmonary circulation will impact the exhalation profile, and several recent mathematical models have attempted to describe these dynamics (Hyde et al., 1997;

Tsoukias and George, 1998). These models have assumed a constant $D_{\rm LNO}$ for simplicity and for a lack of adequate description of $D_{\rm LNO}(V_{\rm A})$. The development and predictions of these models will have to be reexamined using the new information presented in this manuscript.

5. Conclusions

The experimental data combined with the use of a new mathematical model in this manuscript suggest that current methods for determining $D_{\rm L}$ need to be reexamined. By including the effects of sequential filling during inflation and the volume dependence of $D_{\rm L}$ in our analysis, we conclude that the current clinically accepted Jones-Meade Method may significantly underestimate $D_{\rm L}$. In addition, if the Jones-Method is used to determine the volume dependence of $D_{\rm L}$ using multiple breathing maneuvers, the technique will underestimate this dependence. This conclusion is based on our experimental data that suggest the normal lung inflates, in part, sequentially, and that $D_{\rm L}$ for both CO and NO is a positive function of V_A. The new model and technique are simple to use (a single exhalation) and are not constrained by as many experimental conditions as the Jones-Meade Method such as a rapid inhalation and exhalation relative to the breathhold time. The robustness of the model needs further testing under a larger range of experimental conditions, and also must be applied to patients who suffer from lung diseases that are commonly assessed by changes in $D_{\rm L}$.

Acknowledgements

This manuscript was supported by grants from the National Institutes of Health (R29 HL60636) and the National Science Foundation (BES-9619340).

References

ATS, 1987. Single breath carbon monoxide diffusing capacity

- transfer factor. Recommendations for a standard technique. Statement of the American Thoracic Society. Am. Rev. Respir. Dis. 136, 1299–307.
- Badavas, P.C., Saridis, G.W., 1970. Responce identification of distributed systems with noisy measurements at finite points. Inf. Sci., 19–34.
- Beck, T.J., Arnold, K.T., 1977. Parmeter Estimation in Engineering and Science. Wiley, New York.
- Bischof, C., Carle, A., Khademi, P., Mauer, A., 1994. The ADIFOR 2.0 system for the automatic differentiation of FORTRAN 77 programs. Technical Report ANL-MCS-P481-1194. Argonne National Laboratory.
- Borland, C.D.R., Higenbottam, T.W., 1989. A simultaneous single breath measurement of pulmonary diffusing capacity with nitric oxide and carbon monoxide. Eur. Respir. J. 2, 56–63.
- Chatterjee, S., Price, B., 1977. Regression Analysis by Example. John Wiley and Sons.
- Cotton, D.J., Newth, C.J., Portner, P.M., et al., 1979. Measurement of single-breath CO diffusing capacity by continuous rapid CO analysis in man. J. Appl. Physiol. 46, 1149–1156.
- Dollfuss, R.E., Milic-Emili, J., Bates, D.V., 1967. Regional ventilation of the lung studied with boluses of ¹³³xenon. Respir. Physiol. 2, 234–246.
- Frank, P.M., 1978. Introduction to Systems Sensitivity Theory. Academic Press, New York.
- Graham, B.L., Dosman, J.A., Cotton, D.J., 1980. A theoretical analysis of the single breath diffusing capacity for carbon monoxide. IEEE Trans. Biomed. Eng. 27, 221–227.
- Guenard, H., Varene, N., Vaida, P., 1987. Determination of lung capillary blood volume and membrane diffusing capacity in man by the measurements of NO and CO transfer. Respir. Physiol. 70, 113–120.
- Hyde, R.W., Geigel, E.J., Olszowka, A.J., 1997. Determination of production of nitric oxide by lower airways-theory. J. Appl. Physiol. 82, 1290–1296.
- Jones, R.S., Meade, F., 1961. A theoretical and experimental analysis of anomalies in the estimation of pulmonary diffusing capacity by the single breath method. Quart. J. Exp. Physiol. 46, 131–143.
- Kahaner, D., Moler, C., Nash, S., 1988. Numerical Methods and Software. Prentice Hall, New Jersey.
- Kharitonov, S., Alving, K., Barnes, P.J., 1997. Exhaled and nasal nitric oxide measurements: recommendations. The European Respiratory Society Task Force. Eur. Respir. J. 10, 1683–1693.
- Krogh, M., 1915. The diffusion of gases through the lungs of man. J. Physiol. London 49, 271–300.
- Martonen, T.B., Wilson, A.F., 1982. Theoretical basis of single breath gas absorption tests. J. Math. Biol. 14, 203–220.
- Newth, C.J., Cotton, D.J., Nadel, J.A., 1977. Pulmonary diffusing capacity measured at multiple intervals during a single exhalation in man. J. Appl. Physiol. 43, 617– 625.

- Ogilvie, C.M., Forster, R.E., Blakemore, W.S., et al., 1957. A standarized breath holding technique for the clinical measurement of the diffusing capacity of the lung for carbon monoxide. J. Clin. Invest. 36, 1–17.
- Staub, N.C., 1969. Respiration. Annu. Rev. Physiol. 31, 173-202.
- Tsoukias, N.M., 1999. Characterization of nitric oxide exchange in human lungs. Ph.D. Dissertation. University of California, Irvine.
- Tsoukias, N.M., George, S.C., 1998. A two-compartment

- model of pulmonary nitric oxide exchange dynamics. J. Appl. Physiol. 85, 653-666.
- Tsoukias, N.M., Wilson, A.F., George, S.C., 2000. Effect of alveolar volume and sequential filling on the diffusing capacity of the lungs: I. Theory. Respir. Physiol. 120, 231–249.
- Weibel, E.R., Untersee, P., Gil, J., et al., 1973. Morphometric estimation of pulmonary diffusion capacity. VI. Effect of varying positive pressure inflation of air spaces. Respir. Physiol. 18, 285–308.